Lunar Impact History from $^{40}Ar/^{39}Ar$ Dating of Glass Spherules

Timothy S. Culler,[1,3] Timothy A. Becker,[4*] Richard A. Muller,[2,3*] Paul R. Renne[1,4*†]

Lunar spherules are small glass beads that are formed mainly as a result of small impacts on the lunar surface; the ages of these impacts can be determined by the $^{40}Ar/^{39}Ar$ isochron technique. Here, 155 spherules separated from 1 gram of Apollo 14 soil were analyzed using this technique. The data show that over the last ~3.5 billion years, the cratering rate decreased by a factor of 2 to 3 to a low about 500 to 600 million years ago, then increased by a factor of 3.7 ± 1.2 in the last 400 million years. This latter period coincided with rapid biotic evolutionary radiation on Earth.

The frequency of impact cratering on planets and satellites over the history of the solar system is important in understanding the dynamics of planetesimals in the early solar system and the evolution of terrestrial life. Much of this history is poorly constrained because plate tectonics, erosion, and sedimentation have eliminated many of the craters older than a few hundred million years on Earth. Consequently, we have turned to the moon to elucidate the history of impacts in the inner solar system. The relative quiescence of the moon allows the impact record to be preserved in a nearly pristine state.

The Apollo missions returned samples that allowed the formation of lunar maria to be dated. Crater counts on these surfaces yielded average cratering rates from ~4.0 to 3.2 billion years ago (Ga), but this period represents less than one-fourth of the 4.5-billion-year (Gy) history of impacts on Earth and the moon (*1, 2*). A handful of exotic lunar samples have been dated and correlated to young craters such as Tycho (*3*), Copernicus (*4*), and Autolycus (*5*), and these have placed rough constraints on the last 3 Gy of cratering history. The existing data suggest that the crater production rate has been constant to within a factor of 2 to 4 (*1, 2, 5–8*) over this time. However, measurements of recent crater production rates on the moon (*9*) and Earth (*10, 11*), as well as some astronomical surveys (*12, 13*), suggest that the cratering rate over the last 0.5 to 1 Gy has increased by a factor of about 2 relative to earlier rates.

The present study was undertaken to refine our knowledge of lunar cratering rates over the last ~3.8 Gy, to test the inferred recent increase in crater production, and to evaluate whether known terrestrial impacts and other events coincided with pulses of cratering in the inner solar system. We dated lunar glass spherules using the $^{40}Ar/^{39}Ar$ technique, as suggested by Muller (*14*). The spherules were formed in lunar impacts and volcanic eruptions; they are abundant in all of the Apollo soil samples (*15*) and are sufficiently small (150 to 250 μm in diameter) that they likely have degassed accumulated pre-impact radiogenic ^{40}Ar upon melting (*16*). It is possible to distinguish impact spherules from those formed in pyroclastic eruptions on the basis of their composition (in particular their Mg/Al ratio), the presence of melt splashes and volatile coatings on the spherules, and the ferromagnetic resonance intensity of individual spherules (*17–19*). Earlier work by us (*17*) and others (*18, 19*) has led us to conclude that the majority of spherules at typical landing sites (including Apollo 14) are formed in impacts, and that most of them came from different impacts. By dating these spherules, we can determine the age of the impacts that formed them (*14, 20*).

The spherules from an Apollo 11 soil sample are compositionally similar (with some exceptions) to the locally exposed rocks, which suggests that the majority of impact spherules are formed in small impacts proximal to their collection locality (*17*). This observation led us to choose spherules from the Apollo 14 mission (which landed on the Fra Mauro formation) as the most appropriate for accurate $^{40}Ar/^{39}Ar$ dating, because the regolith from this site is enriched in K by a factor of 5 to 10 relative to that at other Apollo landing sites.

We dated 155 spherules using the $^{40}Ar/^{39}Ar$ isochron technique (*21*). The $(^{40}Ar/^{36}Ar)_{trapped}$ ratios vary from 0.02 ± 0.13 to 3.54 ± 0.62 (Fig. 1) (*22*). The variations may reflect variations in isotopic composition of the solar wind or "orphan" ^{40}Ar (*23*), although no straightforward correlation is apparent between isochron age and initial $^{40}Ar/^{36}Ar$.

Our data show that the spherule production rate from 3.5 Ga to the present was not constant (Fig. 2). Although this result contradicts most conclusions by previous workers (*1, 2*), Fig. 3

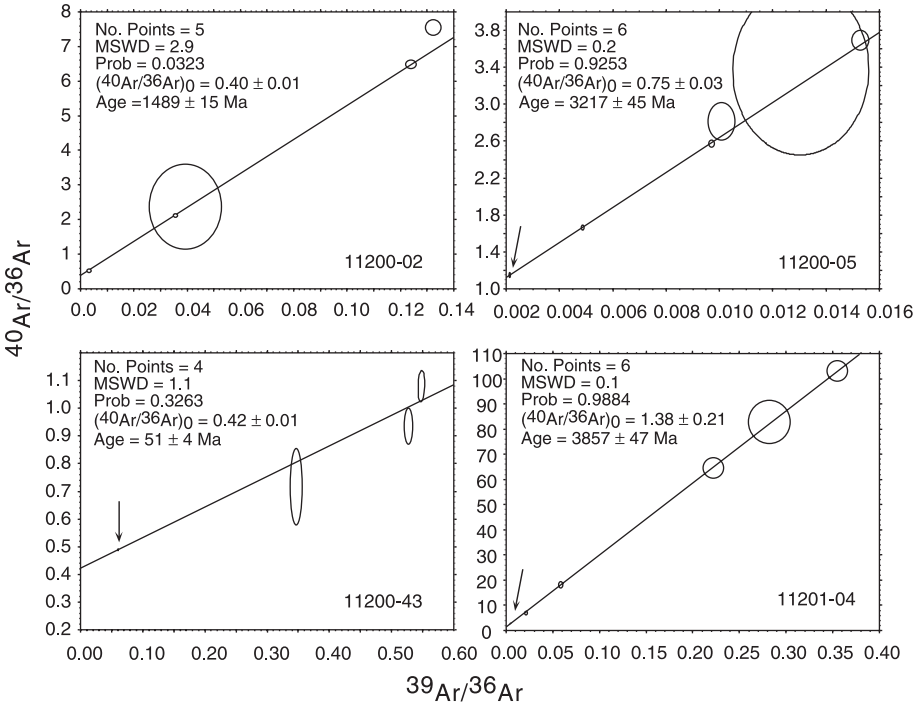

Fig. 1. $^{40}Ar/^{39}Ar$ isotope correlation diagrams (isochrons), yielding age and $(^{40}Ar/^{36}Ar)_{trapped}$ ratio from 4 of the 155 spherules. Note that several of the error ellipses (indicated by arrows) in the diagrams are smaller than the line defining the isochron (*22*).

[1]Department of Geology and Geophysics, [2]Department of Physics, University of California, Berkeley, CA 94720, USA. [3]Lawrence Berkeley National Laboratory, Berkeley, CA 94720, USA. [4]Berkeley Geochronology Center, 2455 Ridge Road, Berkeley, CA 94709, USA.

*These authors are listed alphabetically.
†To whom correspondence should be addressed. E-mail: prenne@bgc.org

Downloaded from http://science.sciencemag.org/ on August 14, 2016

shows that it is within the uncertainty limits determined by the Basaltic Volcanism Study Project (BVSP) (*1*). The production rate from 4.0 to 3.0 Ga was roughly twice the production rate from 2.0 to 0.5 Ga, and there is an increase in the spherule production rate beginning about 0.4 Ga (Fig. 2). The reduced spherule production for ages older than 3.5 Ga is likely due to the effect of lunar gardening combined with the age of the Fra Mauro formation (3.85 Ga) (*7*). The appearance of the peak in spherule numbers in the 2.8- to 3.2-Ga bin (25 events) rather than in the 3.2- to 3.6-Ga bin (20 events) may be due to a statistical fluctuation. If we include only those spherules whose age uncertainty is ≤0.1 Ga, then the maximum counts occur in the 0- to 0.4-Ga bin (14 events) and in the 3.6- to 4.0-Ga bin (10 events).

There are two potential systematic biases that could cause an apparent increase in the recent cratering rate, and we investigated these to determine whether the increase since 0.4 Ga is related to a sampling bias. Both biases come from the proximity of Cone crater, a young [25 million years old (Ma)] and relatively large (diameter 370 m, depth 75 m) crater located about 1 km from our sample collection site (*7*). Calculations by McGetchin *et al.* (*24, 25*) and seismic data from Chao (*26*) indicate that there is an ejecta layer from Cone crater, 10 to 50 cm thick, at our sample location. Because our sample was scooped from the "upper several centimeters" of regolith (*27*), it consists almost entirely of Cone crater ejecta. This ejecta is well mixed (hence no gardening correction should be applied) and, because Cone crater is much deeper than the local regolith [which is about 8 m deep (*7*)], our sample of this ejecta contains spherules that represent the entire cratering history in the vicinity of the landing site.

The first potential bias that could cause the 0.4-Ga increase is the possibility of excess spherules produced in the Cone impact. Eleven spherules between 0 and 0.4 Ga fall within 1σ of the Cone crater age. There is no correlation between the color of the spherules and the younger ages. Of these 11 spherules, 3 (of 85) are black, 3 (of 36) are yellow, 3 (of 10) are orange, 1 (of 9) is green, and 1 (of 2) is white. If we assume that all 11 spherules are due to Cone crater, the youngest histogram bin in Fig. 2 is reduced from 26 to 15 and a factor of ~2 enhancement in cratering rate beginning at 0.4 Ga is still present. Hence, we conclude that the recent peak in spherule production rates is not entirely due to spherules from Cone crater.

A second possible bias may result from a thin layer of material younger than the Cone impact. The ejecta blanket from Cone crater consists of well-mixed regolith ranging in age from the Cone impact (25 Ma) to the emplacement of the Fra Mauro formation (~3.85 Ga). If a thin veneer of material younger than Cone crater was emplaced on top of the Cone ejecta blanket, we would sample a disproportionate amount of young material, which would in turn bias our sample distribution toward ages younger than Cone crater. To test for this bias, we have removed spherules within 1σ of the Cone crater age (i.e., 0 to 25 Ma). These happen to be the same 11 considered above as potential spherules from the Cone impact and, when removed, show that an increase is still present.

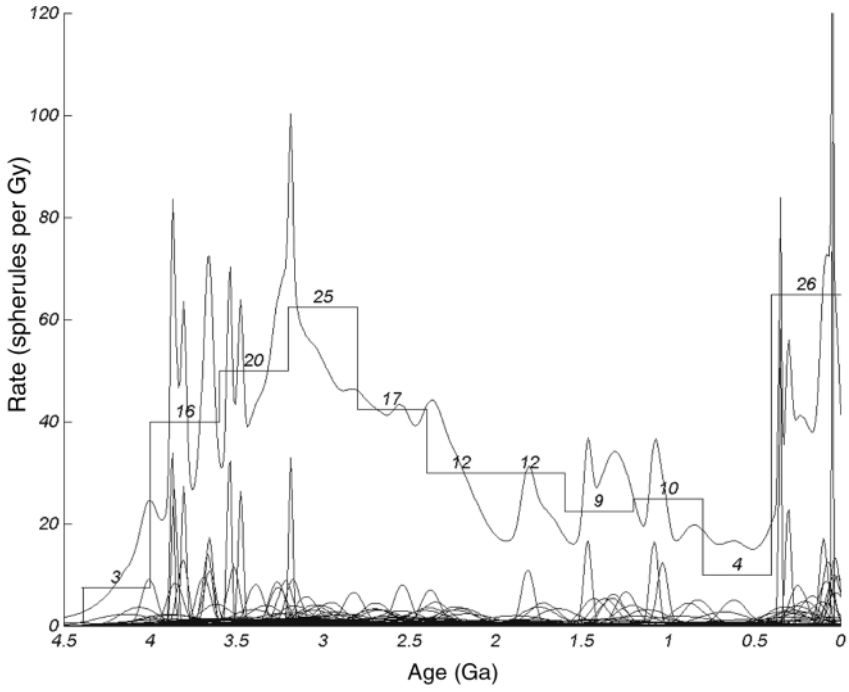

Fig. 2. Age distribution of 155 spherules. Each Gaussian near the bottom of the plot represents a single spherule; its width corresponds to the 1σ error in its age uncertainty, and each Gaussian has the same area. Therefore, spherules with precise age determinations have high, narrow Gaussians and spherules with poor age determinations have low, wide Gaussians. The smooth, continuous line is an ideogram created by summing the Gaussians. Also shown is a histogram of the data with 0.4-Gy bins normalized to the number of spherules formed per billion years; numbers above histogram bins indicate the number of spherules in that bin. Both the ideogram and histogram show a significant decrease in cratering from 3.0 to 0.5 Ga and a factor of nearly 4 increase in cratering over the last 0.4 Ga. We believe that the ideogram, because it takes into account the uncertainties in the age determinations, represents the best statistical estimate of the cratering rate, although spikes caused by a single, well-dated spherule should be disregarded. Because the histogram allows the easiest estimate of statistical significance, both are shown.

The median error in our age uncertainties is ±0.15 Ga (1σ). Therefore, in any given 0.4-Ga period we expect about 40% of the spherules to agree within error with any given age. In the youngest bin in Fig. 2 there are 26 spherules, so 7 to 11 spherules should agree with the age of Cone crater. The fact that we see 11 spherules implies that there is not an unusual frequency of spherules consistent with that age.

Because few if any excess spherules were produced from the Cone impact and a thin veneer of post–Cone crater material cannot completely account for the excess of spherules younger than 0.4 Ga, we conclude that the apparent increase in spherule production over the last 0.4 Ga is real. Repeating these experiments with soil samples from other Apollo landing sites would enable us to test whether Cone crater (or any other local event) is unduly biasing our data.

To determine the magnitude of this increase, we compared the number of spherules in the youngest 0.4-Gy bin (Fig. 2), which contains 26 ± 5.1 events, with the average of the second and third youngest bins, from the period 1.2 to 0.4 Ga. These bins contain an average of 7 ± 1.9 events. The nominal increase in cratering rate is (26 ± 5.1)/(7 ± 1.9) = 3.7 ± 1.2, and the minimum (and conservative) increase in cratering rate (taken by excluding spherules within 1σ of the Cone crater age bin) is (15 ± 3.9)/(7 ± 1.9) = 2.1 ± 0.8. Because we concluded above that the systematic biases are negligible, our best estimate for the increase in cratering rate is 3.7 ± 1.2.

Previous estimates of cratering rates have been based on counting craters on dated surfaces (*1, 28*). To compare our rates with these, we plotted these crater counts and the integral of our rate estimate (the number of spherule ages less than a given age) (Fig. 3). These previous estimates do not show any evidence of the 0.4-Ga increase in cratering rate, and it is impossible to distinguish a

Downloaded from http://science.sciencemag.org/ on August 14, 2016

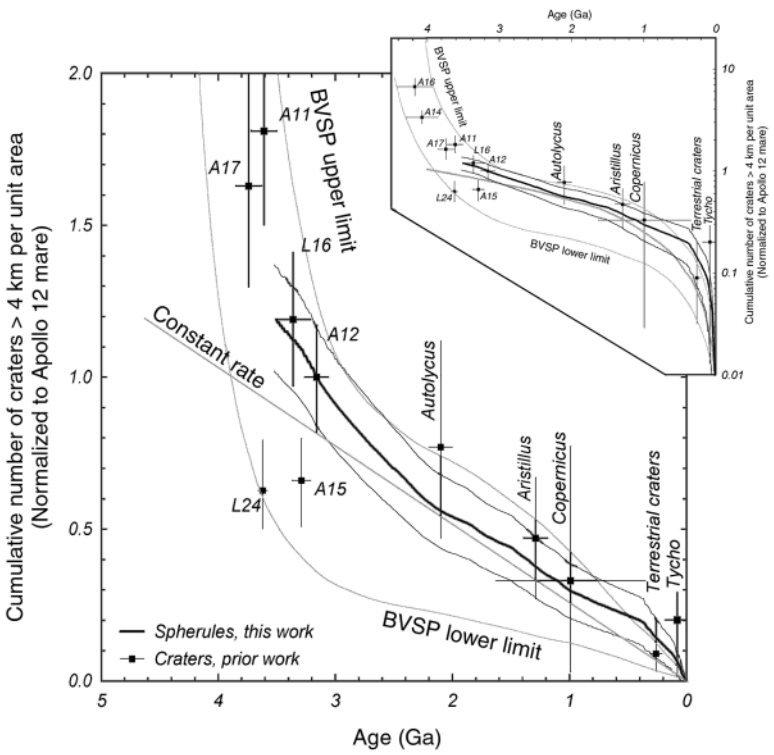

Fig. 3. Cumulative numbers of craters versus time, as calculated from spherule production rate and shown on both a logarithmic scale (upper right) and a linear scale. All crater production rates are normalized to unity at 3.16 Ga, the age of the Apollo 12 mare (they are forced to have a crater production rate of 1 at this age). The thick black line shows the results calculated from our data by integrating our crater frequency measurements (thin black lines indicate 1σ uncertainties). The thick gray line shows previous results from crater frequency measurements (thin gray lines are estimates of 1σ uncertainties). Ages of the mare units, Copernicus, Tycho, and terrestrial craters are taken from (*1*). Ages of Autolycus and Aristillus are taken from (*5*); we converted their D_L values to cumulative crater frequencies using figure 8.8.6 in (*1*). Changes in cratering rate appear as changes in slope.

factor of 2 to 3 decrease over the period 3.5 to 0.5 Ga in the crater counting data because of the large uncertainties. It is important to note that most spherules are probably formed in small impacts (*17*), whereas measurements based on crater counting techniques reflect cratering rates of large impactors.

The spherule data show that the crater production rate has not been constant over the last 3 Gy, as had been generally assumed (*1, 2, 28*). Our data show that the cratering rate at ~3.0 Ga was two to three times the cratering rate at ~1.0 Ga, in agreement with the conclusions of Ryder *et al.* (*5*). Our data also provide evidence for an increase in the cratering rate over the last 0.4 Gy. The cause of this increase is not known, although McEwen *et al.* had shown evidence for a recent increase in impacts (*9*) and offered a possible reason for it.

Given the present sensitivity of the $^{40}Ar/^{39}Ar$ dating technique, future measurements to extend these results either must be made at sites with high potassium (such as Apollo 14) or must use larger spherules. Spherules from the Apollo 16 landing site on the Descartes highlands could allow measurements of the lunar cratering history further back in time, provided that the sample area has not been covered by ejecta from one of the late basin-forming impacts, such as Imbrium. Such measurements could, in principle, allow us to distinguish between the tail end of planetary accretion and a lunar cataclysm. If Apollo 16 is covered by basin ejecta, a relatively inexpensive lunar sample return mission to a site that has not been covered by basin ejecta may be needed to distinguish between the two hypotheses.

Our data show that the lunar cratering rate overall has decreased over the last 3 Gy and has not remained constant. They also show an increase in the cratering rate roughly coincident with the "Cambrian explosion" of complex life on Earth (*29, 30*). Our data do not allow specificity as to the effect that increased cratering may have had on the evolution of terrestrial life, but the correlation is permissible evidence of a causal relation. It is possible that increased debris influx had a net stimulating effect on biotic diversity, despite the occasional occurrence of large impacts with destructive consequences.

References and Notes

1. BVSP, *Basaltic Volcanism on the Terrestrial Planets* (Pergamon, New York, 1981).
2. W. K. Hartmann, *Proceedings of the Conference on the Lunar Highlands Crust*, J. J. Papike, Ed. (Pergamon, Elmsford, NY, 1980), pp. 155–171.
3. R. J. Drozd, C. M. Hohenberg, C. J. Morgan, F. A. Podosek, M. L. Wroge, *Proc. Lunar Sci. Conf.* **8**, 3027 (1977).
4. H. A. Pohn, U.S. Geological Survey Map I-627 [ORB III-9(100)] (1971).
5. G. Ryder, D. Bogard, D. Garrison, *Geology* **19**, 143 (1991).
6. W. K. Hartmann, *Astrophys. Space Sci.* **17**, 48 (1972).
7. D. E. Wilhelms, *U.S. Geol. Surv. Prof. Pap. 1348* (1987), p. 302.
8. G. Neukum and B. A. Ivanov, in *Hazards Due to Comets and Asteroids*, T. Gehrels, Ed. (Univ. of Arizona Press, Tucson, AZ, 1994), pp. 359–416.
9. A. S. McEwen, J. M. Moore, E. M. Shoemaker, *J. Geophys. Res.* **102**, 9231 (1997).
10. E. M. Shoemaker, R. J. Hackman, R. E. Eggleton, *Adv. Astronaut. Sci.* **8**, 70 (1963).
11. R. A. F. Grieve and E. M. Shoemaker, in *Hazards Due to Comets and Asteroids*, T. Gehrels, Ed. (Univ. of Arizona Press, Tucson, AZ, 1994), pp. 417–462.
12. E. M. Shoemaker, R. F. Wolfe, C. S. Shoemaker, *Geol. Soc. Am. Spec. Pap. 247* (1990), p. 155.
13. E. M. Shoemaker, P. R. Weissman, C. S. Shoemaker, in *Hazards Due to Comets and Asteroids*, T. Gehrels, Ed. (Univ. of Arizona Press, Tucson, AZ, 1994), pp. 313–336.
14. R. A. Muller, *Tech. Rep. LBL-34168* (Lawrence Berkeley National Laboratory, Berkeley, CA, 1993).
15. B. P. Glass, *Introduction to Planetary Geology* (Cambridge Univ. Press, New York, 1982).
16. G. B. Dalrymple, G. A. Izett, L. Snee, J. D. Obradovich, *U.S. Geol. Surv. Bull.* **2065**, 20 (1993).
17. T. S. Culler and R. A. Muller, in preparation.
18. D. S. McKay and G. H. Heiken, *EOS* **54**, 599 (1973).
19. C. D. Stone, L. A. Taylor, D. S. McKay, R. V. Morris, *Proc. Lunar Planet. Sci. Conf.* **13** (suppl. 1), A182 (1982).
20. T. S. Culler, R. A. Muller, P. Renne, *Proc. Lunar Planet. Sci. Conf.* **27**, 279 (1996).
21. Each of the 155 Apollo 14 spherules was hand-picked from the 14163 soil sample, cleaned, and sorted according to color into one of six categories: black/opaque (85 total spherules), yellow (36), gray (13), orange/red (10), green (9), and white (2). These variations in color are thought to relate to the concentration of titanium and, to a lesser extent, iron in the glass of the spherules [C. Frondel, C. J. Klein, J. Ito, J. C. Drake, *Proc. Lunar Planet. Sci. Conf.* **1**, 445 (1970)]. Each color group was placed in a separate pit in an aluminum irradiation disk along with MMhb-1 [S. D. Samson and E. C. Alexander, *Chem. Geol.* **66**, 27 (1987)] and FCs (*31*) fast neutron fluence monitors (standards). The samples underwent ~100 hours of irradiation at the Oregon State University Reactor (fast neutron fluence parameter $J = 0.0261 \pm 0.001$). We used the cadmium-lined in-core instrument transfer facility, which virtually eliminates thermal neutron reactions such as $^{37}Cl(n,\gamma)^{38}Ar$ and $^{40}K(n,p)^{40}Ar$. Correction factors for interfering isotopes (*31*) are $(^{36}Ar/^{37}Ar)_{Ca} = (2.64 \pm 0.02) \times 10^{-4}$, $(^{39}Ar/^{37}Ar)_{Ca} = (7.04 \pm 0.06) \times 10^{-4}$, and $(^{40}Ar/^{39}Ar)_K = (8 \pm 3) \times 10^{-4}$. Mass discrimination is monitored by periodic analyses of air pipettes. Each spherule was degassed stepwise by an 8-W Ar-ion laser in 5 to 30 steps, depending on the size and potassium concentration of the spherule. The extraction line we used has a cryo-trap operated at −122°C to remove condensable gases and two SAES C-50 getters (one was turned off to lower instrument blanks). Isotopic analyses were done with a MAP 215 noble gas mass spectrometer. The laser, extraction line, and mass spectrometer are all fully automated. Because the initial isotopic composition of Ar in the spherules cannot be assumed, our analytical strategy focused on step-heating to generate data, facilitating the use of $^{40}Ar/^{36}Ar$ versus $^{39}Ar/^{36}Ar$ isochrons. This approach relies on releasing gas comprising binary mixtures of initial Ar (of uniform isotopic composition) with radiogenic Ar ($^{40}Ar^*$). In most cases, low laser power steps are enriched in a low $^{40}Ar/^{36}Ar$ component, whereas heating at higher power produced higher $^{40}Ar/^{36}Ar$ because of the release of proportionately more $^{40}Ar^*$. In some cases, additional

Downloaded from http://science.sciencemag.org/ on August 14, 2016

components of Ar were clearly associated with anomalous Ca/K (determined from $^{37}Ar/^{39}Ar$), which we construe to reflect Ca-rich clasts that were incompletely degassed during impact melting; we excluded such analyses from isochron regressions. In some other cases, more than two components of Ar are indicated by nonlinear scatter on isochron diagrams. In such cases the age error is multiplied by the square root of the mean squared weighted deviates, such that isochron ages with excess scatter are deweighted and have little impact on our conclusions. Terrestrial atmospheric contamination is efficiently removed in sample cleaning and preanalysis bakeout, as indicated by consistently low $^{40}Ar/^{36}Ar$ in even the lowest temperature extraction steps and by the linearity of the isochron data.

22. Summary data for all isochron ages are available at *Science* Online (www.sciencemag.org/feature/data/1044416.shl).
23. P. Eberhardt, *Proc. Lunar Planet. Sci. Conf.* **3**, 1821 (1972).
24. T. R. McGetchin, M. Settle, J. W. Head, *Earth Planet. Sci. Lett.* **20**, 226 (1973).
25. G. H. Heiken, T. Vaniman, B. French, Eds., *Lunar Sourcebook* (Cambridge Univ. Press, New York, 1991).
26. E. C. T. Chao, *USGS J. Res.* **1**, 1 (1973).
27. R. V. Morris, R. Score, C. Dardano, G. Heiken, *Tech. Rep. JSC 19069* (Lyndon B. Johnson Space Center, 1983).
28. F. Hörz, R. Grieve, G. H. Heiken, P. Spudis, A. Binder, in *Lunar Sourcebook*, G. H. Heiken, T. Vaniman, B. French, Eds. (Cambridge Univ. Press, New York, 1991), pp. 285–356.
29. J. P. Grotzinger, S. A. Bowring, B. Z. Saylor, A. J. Kaufman, *Science* **270**, 598 (1995).
30. J. P. Grotzinger, *Am. Assoc. Petrol. Geol.* **18**, 1954 (1997).
31. P. R. Renne *et al.*, *Chem. Geol. (Isot. Geosci. Sect.)* **145**, 117 (1998).

32. Supported by the Ann and Gordon Getty Foundation. We thank W. Alvarez, A. Deino, J. Donovan, D. Karner, K. Ludwig, and T. Teague for discussions and various other invaluable contributions to this research, K. Nishiizumi for curating the samples, and NASA for providing them.

11 August 1999; accepted 18 January 2000

Internal Structure and Early Thermal Evolution of Mars from Mars Global Surveyor Topography and Gravity

Maria T. Zuber,[1,4]* Sean C. Solomon,[2] Roger J. Phillips,[3] David E. Smith,[4] G. Leonard Tyler,[5] Oded Aharonson,[1] Georges Balmino,[6] W. Bruce Banerdt,[7] James W. Head,[8] Catherine L. Johnson,[2] Frank G. Lemoine,[4] Patrick J. McGovern,[2]† Gregory A. Neumann,[1,4] David D. Rowlands,[4] Shijie Zhong[1]

Topography and gravity measured by the Mars Global Surveyor have enabled determination of the global crust and upper mantle structure of Mars. The planet displays two distinct crustal zones that do not correlate globally with the geologic dichotomy: a region of crust that thins progressively from south to north and encompasses much of the southern highlands and Tharsis province and a region of approximately uniform crustal thickness that includes the northern lowlands and Arabia Terra. The strength of the lithosphere beneath the ancient southern highlands suggests that the northern hemisphere was a locus of high heat flow early in martian history. The thickness of the elastic lithosphere increases with time of loading in the northern plains and Tharsis. The northern lowlands contain structures interpreted as large buried channels that are consistent with northward transport of water and sediment to the lowlands before the end of northern hemisphere resurfacing.

The interior structure of Mars contains information on bulk composition, differentiation and melting history, and mantle dynamics, all of which bear on the planet's thermal evolution. Global models of martian topography from the Mars Orbiter Laser Altimeter (MOLA) (*1*) and gravity from Doppler tracking (*2*) obtained during the mapping mission of the Mars Global Surveyor (MGS) spacecraft (*3*) have now achieved the coverage and quality required for the first reliable determination of Mars's crustal and upper mantle structure.

We analyzed updated models of topography (*4*) (Fig. 1A) and free-air gravity (*5*) (Fig. 1B) expanded to spherical harmonic degree and order 60, corresponding to a spatial resolution of ~178 km. Global correlations of the fields are shown in Web figure 1 (*6*). To investigate the martian internal mass distribution, we calculated Bouguer gravity anomalies, for which the gravitational attraction of surface topography is subtracted from the free-air gravity field to reveal the subsurface mass distribution. Bouguer gravity anomalies have been calculated for Mars, but the uncertainties limited geophysical interpretation (*7*).

The simplest interpretation of the Bouguer gravity is that subsurface mass variations are a consequence of variations in the thickness of a crust of uniform density. This interpretation provides a first-order indication of Mars's internal structure but does not account for density variations within the crust or upper mantle. A model based on this premise provides an approximate lower limit on mean crustal thickness and volume (*8*). In this model, a crust of density 2900 kg m^{-3} has an average thickness of 50 km and represents 4.4% of Mars's volume (Fig. 1C). The minimum thickness is 3 km beneath the Isidis basin, and the maximum thickness of 92 km occurs in the Syria Planum region of Thaumasia.

The major features in the free-air gravity field (Fig. 1B) include a broad but geometrically complex anomaly associated with the Tharsis province, positive gravity anomalies over large volcanoes, localized mass concentrations centered on large impact basins, and mass deficits (negative anomalies) associated with the Valles Marineris canyon system. Aside from these structures, the gravitational field is relatively smooth (*9*). As a consequence, the crustal thickness map, to first order, correlates with the principal features of surface topography (Fig. 1A). The primary topographic feature on Mars is the global south-to-north slope (*10*, *11*). Cross sections of crustal structure (Fig. 2) indicate a progressive thinning of the crust from high southern latitudes toward the north. The northward slope and corresponding decrease in crustal thickness continue through the Tharsis province (Fig. 2B), but the crustal structure changes to a zone of approximately uniform thickness (~35 to 40 km, except for buried basins) under the northern lowlands and the Arabia Terra region of the southern highlands (Fig. 2A). On the basis of their similarity in crustal structure, we infer that Arabia Terra is related to the northern lowlands and may represent exposed basement of the resurfaced northern plains.

The transition between the major crustal

[1]Department of Earth, Atmospheric, and Planetary Sciences, Massachusetts Institute of Technology, Cambridge, MA 02139, USA. [2]Department of Terrestrial Magnetism, Carnegie Institution of Washington, Washington, DC 20015, USA. [3]Department of Earth and Planetary Sciences, Washington University, St. Louis, MO 63130, USA. [4]Earth Sciences Directorate, NASA/Goddard Space Flight Center, Greenbelt, MD 20771, USA. [5]Center for Radio Astronomy, Stanford University, Stanford, CA 94035–9515, USA. [6]Groupe de Recherches de Geodesie Spatiale, Toulouse, France. [7]Jet Propulsion Laboratory, Pasadena, CA 91109, USA. [8]Department of Geological Sciences, Brown University, Providence, RI 02912, USA.

*To whom correspondence should be addressed. E-mail: zuber@mit.edu

†Present address: Lunar and Planetary Institute, Houston, TX 77058. USA.

Downloaded from http://science.sciencemag.org/ on August 14, 2016

Science
AAAS

Lunar Impact History from $^{40}Ar/^{39}Ar$ Dating of Glass Spherules

Timothy S. Culler, Timothy A. Becker, Richard A. Muller and Paul R. Renne (March 10, 2000)

Science **287** (5459), 1785-1788. [doi: 10.1126/science.287.5459.1785]

Editor's Summary

This copy is for your personal, non-commercial use only.

Article Tools Visit the online version of this article to access the personalization and article tools:
http://science.sciencemag.org/content/287/5459/1785

Permissions Obtain information about reproducing this article:
http://www.sciencemag.org/about/permissions.dtl

Downloaded from http://science.sciencemag.org/ on August 14, 2016

Science (print ISSN 0036-8075; online ISSN 1095-9203) is published weekly, except the last week in December, by the American Association for the Advancement of Science, 1200 New York Avenue NW, Washington, DC 20005. Copyright 2016 by the American Association for the Advancement of Science; all rights reserved. The title *Science* is a registered trademark of AAAS.